Research Article

Junjie Sheng#, Yujun Ji#, Shijie Zhao, Yong Qiu*, Chun Zhao, Gangqiang Tang, and Yanjie Wang*

A radiation-resistant MWCNT/Nafion/MWCNT composite film for humidity perception

https://doi.org/10.1515/epoly-2023-0168
received October 30, 2023; accepted December 07, 2023

Abstract: Humidity is a necessary detection index in the nuclear industry, but the current humidity sensor is unable to resist nuclear radiation. In this work, we develop a radiation-resistant humidity sensor, which is made of multiwalled carbon nanotube (MWCNT)/Nafion/MWCNT composite film. The voltage response of the composite membrane under different relative humidity was measured before and after irradiation in different environments. The results show that in the radiation atmosphere of 21% O_2, MWCNTs were significantly aggregated and fractured, and the number of oxygen functional groups on the surface of the composite membrane increased, resulting in the attenuation of the elastic modulus and a significant decrease in the voltage response and response rate. However, the humidity and structural properties of the composite films did not change significantly after irradiation in a 100% N_2 radiation atmosphere. It is confirmed that the composite film has good radiation resistance in the absence of oxygen.

Keywords: humidity sensors, nuclear radiation, Nafion, multiwalled carbon nanotubes, composite film

1 Introduction

As an important environmental factor, humidity is critical for production and daily life. The humidity sensor is generally composed of humidity-sensitive material, conversion element, and signal conversion circuit, in which the humidity-sensitive material responds directly to the measured humidity. Over the past decades, various sensing materials, including macromolecule compounds (1–6), semiconducting materials (7–13), and porous ceramics (14–18), have been explored to detect humidity. However, humidity sensors made from these materials lack radiation resistance, which limits their practical applications in nuclear radiation environment.

Therefore, a kind of humidity sensing material that can resist radiation for humidity sensors should be developed. In recent years, researchers have developed metal nanocomposites possessing radiation resistance properties. Kim et al. (19) developed high-strength V-graphene nanolayers that were demonstrated to have an excellent radiation tolerance as revealed by the He (+) irradiation study. Si et al. (20) found that the radiation tolerance can be significantly improved by inserting single-layer graphene into tungsten nanofilms. Compared to the metal nanocomposite, carbon nanotube materials have exhibited excellent molecular adsorption properties and are radiation resistant due to their large specific surface area, hollow geometry, high aspect ratio, and the combination of excellent thermal, electrical, and mechanical properties. Al-Haik et al. (21) studied single carbon nanotubes/polyethylene (PE) composites for using in radiation shielding applications. The results suggest that the adhesion between the zigzag, armchair carbon nanotubes (CNTs), and the PE chains outweighs the fragmentation of the polyethylene chains upon irradiation, which exhibits higher structural stabilities and radiation resistance. Li et al. (22) investigated the radiation damage and microstructure evolution of different zigzag single-walled carbon nanotubes subjected to incident carbon ions by molecular dynamics. It was observed that as the incident ion energy increased, the generation of defects reached its maximum. Luo et al. (23) reported a radiation-hardened FET (hybrid CMOS field-effect transistors) that uses semiconducting carbon nanotubes as the channel material, an ion gel as the gate, and poly-imide as the substrate. The FET exhibits a radiation tolerance of up to 15 Mrad at a dose rate of 66.7 rad·s^{-1}, which is notably higher than the tolerance of silicon-based transistors (1 Mrad). Based on the

# These authors contributed equally.

*** Corresponding author: Yong Qiu,** China Academy of Engineering Physics, Mianyang 621900, Sichuan Province, China, e-mail: qiuy@caep.cn
*** Corresponding author: Yanjie Wang,** College of Mechanical & Electrical Engineering, Hohai University, Changzhou 213022, Jiangsu Province, China, e-mail: yjwang@hhu.edu.cn
Junjie Sheng: Institute of Systems Engineering, China Academy of Engineering Physics, Mianyang 621900, Sichuan Province, China
Yujun Ji, Shijie Zhao, Chun Zhao, Gangqiang Tang: College of Mechanical and Electrical Engineering, Hohai University, Changzhou 213022, Jiangsu Province, China

above studies, CNTs are considered to have excellent radiation resistance and can be used to fabricate humidity sensors.

Herein, we developed a multiwalled carbon nanotube (MWCNT)/Nafion/MWCNT composite film with excellent humidity sensing performance, which has good radiation resistance under anaerobic environment. The structure and the microstructure of the inner layer are depicted in Figure 1. The composite film comprises electrode layers on both sides, consisting of multiwalled carbon nanotubes/polyvinylidene fluoride/ionic liquids (MWCNT/PVDF-HFP/ILs), and a core layer in the middle made of perfluorinated sulfonic acid-polytetrafluoroethylene/ionic liquids (Nafion/ILs). When the ambient humidity changes, the cations in Nafion film will absorb or precipitate water molecules. Under the influence of a concentration gradient, ions move to produce electrical signals that are gathered by the acquisition system through the conducting MWCNT film. To study the anti-radiation performance of the composite membrane, the structure and characteristics of the composite membrane and the humidity response performance were tested under different radiation environments (aerobic and anaerobic) and different radiation doses. Finally, we found that the composite film had excellent radiation resistance compared to the aerobic environment in the anaerobic environment and maintained good humidity sensing performance after radiation.

2 Experimental

2.1 Materials

MWCNTs (produced in Nanjing Xianfeng nanotechnology, purity > 95%, specific surface area > 120 $m^2 \cdot g^{-1}$) were 10–20 nm in diameter and 10–20 μm in length. Nafion solution of concentration 20 wt% (produced in DuPont, USA) is composed of perfluorosulfonamide resin, ethanol, and a small amount of other organic solvents. EMI_mBF_4 (1-ethyl-3-methylimidazolium tetrafluoroborate) is used as an ionic liquid. Other reagents include PVDF (produced in Shanghai Aichun Biotechnology Co., Ltd.) and DMAC (*N*,*N*-dimethylacetamide) (produced in Shandong Yousuo Chemical Technology Co., Ltd.).

2.2 Fabrication

Figure 2 shows the preparation process of the MWCNT/Nafion/MWCNT composite film. The first step is the fabrication of the electrolyte core layer. To obtain a bubble-free and uniformly dispersed core layer, 8 g solution composed of 2.4 g Nafion, 0.32 g EMI_mBF_4, and 5.28 g DMAC was cast in the glass mold (an area of 4.5 cm × 4.5 cm) after homogenizing

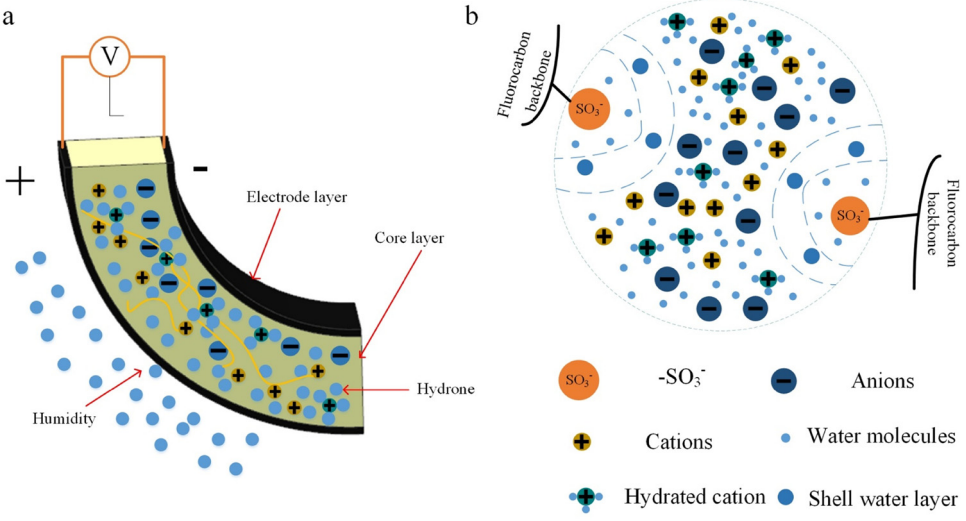

Figure 1: (a) Overall structure of the composite film, schematic diagrams of (b) microchannel inside the composite film.

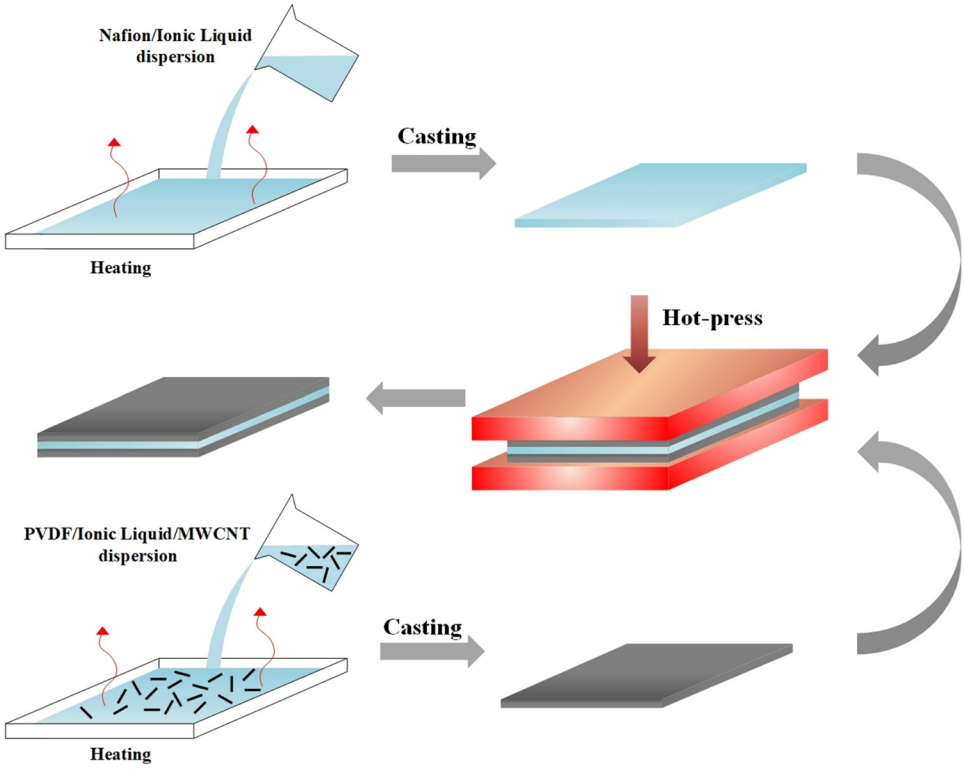

Figure 2: Preparation process of MWCNT/Nafion/MWCNT sensing film.

by magnetic stirrer and completely evaporated in a vacuum drying oven. The second step was the fabrication of the electrode layer. 0.1 g MWCNT, 0.32 g EMI_mBF_4, and 0.2 g PVDF were mixed in 24.5 g DMAC and dispersed in an ultrasonic bath for more than 6 h. Similar to the core layer, the electrode layer was fabricated by casting 10 g of the electrolyte solution in the glass mold (an area of 4.5 cm × 4.5 cm) and completely evaporating the solvent in the vacuum-drying oven. Finally, the two sides of the core layer were tightly combined with two electrode layers by hot pressing to obtain a composite film. The thickness of the composite film was 290–310 μm, which was smaller than the sum of those of two-electrode and one-electrolyte layers, since the thickness of each layer decreased after hot-pressing.

2.3 Characterization

To create a stable humidity environment, the saturated salt solution method was used to obtain gases of varying relative humidity (RH). The selected saturated salt solution in this work and the corresponding RH are shown in Table 1. To achieve a rapid switching of the humidity level, we designed a mini-chamber with a length of 6 cm length and a diameter of 3 cm by 3D printing technology, as shown in Figure 3, which can not only hold a certain amount of humidity gas for exchanging but also easily achieve fast switching from one humidity level to another due to its small volume. A transom is placed within the mini-chamber to ensure that only one side of the composite film detects humidity variation while also preventing gas flow from interfering with the electrical signal produced by the composite film.

The humidity test platform is shown in Figure 4. By exchanging with specific saturated salt solutions, tank A and tank B could obtain different fixed humidity (almost 0% RH, 33% RH, 43% RH, 73% RH, and almost 100% RH), respectively. It should be noted that after 24 h of storage at room temperature, the internal and external exchange balance of the composite membrane is then passed into the gas with the above specific humidity. The room humidity of approximately 57% RH in our laboratory is set as the reference (room temperature is 20°C) for the convenience of testing. There are two check valves installing in the inlet and outlet of the mini chamber to prevent gas backflow and maintain the humidity of the chamber. During the test period, the sample was fixed in the mini-chamber, and the electrical signal generated by the humidity change was transmitted to the PC through an NI acquisition card.

Table 1: Saturated salt solution and corresponding relative humidity (% RH) in humidity generator

Saturated salt solution	Allochroic silicagel	Saturated salt solution (CH_3COOK)	Saturated salt solution ($MgCl_3$)	Saturated salt solution (K_2CO_3)	Saturated salt solution (NaBr)	Saturated salt solution (NaCl)	Saturated salt solution (KCl)	Water
Approximate RH	Almost 0%	23%	33%	43%	57%	73%	84%	Almost 100%

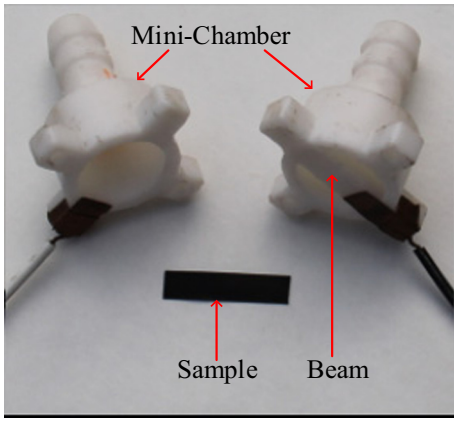

Figure 3: Humidity microchamber.

3 Results and discussion

Figure 5 shows the sheet resistance of the composite film after different radiation processes, which can detect whether there is damage to the MWCNT of the electrode layer. As shown in Figure 5(a), the surface resistance of the composite film before and after radiation was obtained by the four-point probe method. Under 21% O_2 radiation environment, it increased continuously with the increase of dose, reaching 10.3 and 10.92 $\Omega\cdot\square^{-1}$. While the film was exposed to radiation in the absence of oxygen, its surface resistance hardly changed from before irradiation. This indicates that radiation will affect the electrode conductivity of the composite film in an oxygen-containing environment but will not affect it in an oxygen-free environment. Besides, it is observed from Figure 5(b) that the surface resistance of composite film has little change after hot-pressing, which is about 4 $\Omega\cdot\square^{-1}$, exhibiting that the process of hot-pressing does not cause fracture or other damage. However, the surface resistance of the composite film almost increased significantly after 10 and 100 cycles, which might be caused by the volume expansion of the composite film during the adsorption of water particles, leading to the increase in the number of cracks on the surface. The increase in surface resistance is attributed to the breakage of multiwalled carbon nanotubes on the surface, finally resulting in the decrease in conductivity for the composite film.

In addition to measuring the surface resistance, the microstructure of the composite film under different radiation conditions was observed by SEM micrographs. Figure 5(c) shows that the MWCNT of the electrode layer was well dispersed with a diameter of about 10–15 nm, and the surface of the composite membrane had obvious pore structure. Only a few longer MWCNT appeared as aggregates due to Van der Waals' force. Figure 5(d) and (e) shows the microstructure of the composite film under the irradiation

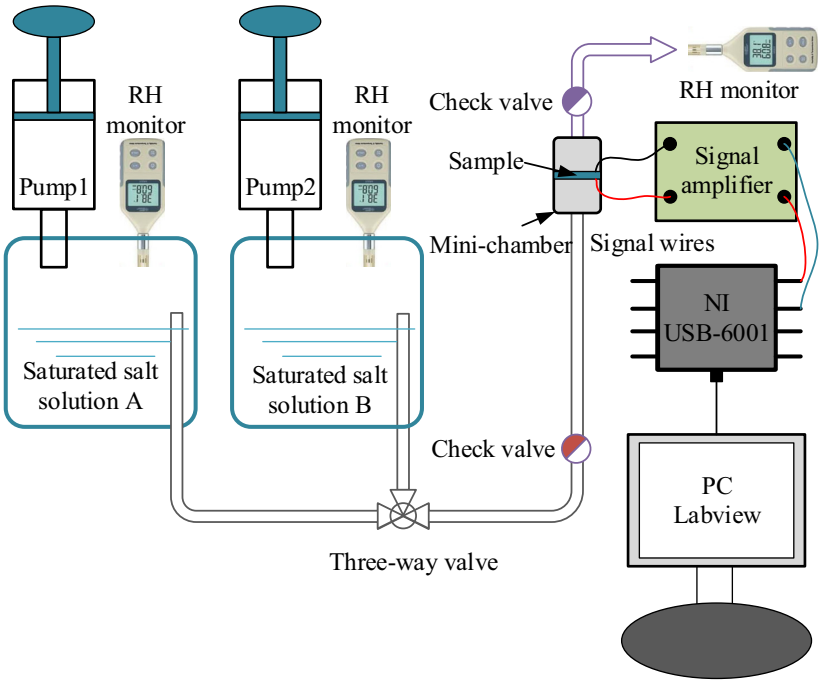

Figure 4: Humidity test platform.

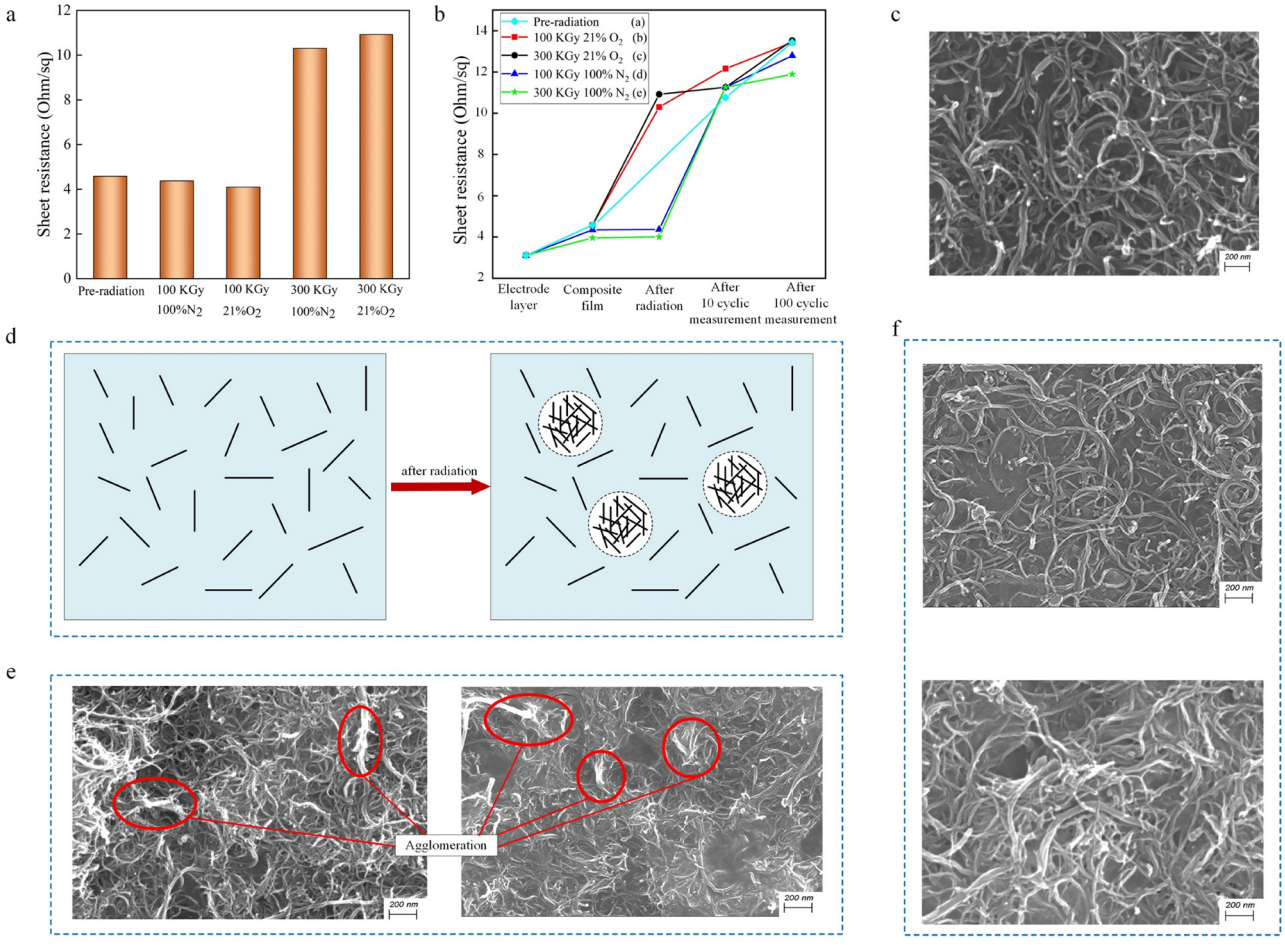

Figure 5: Sheet resistance of the composite film. (a) After different radiations and (b) after different processes. SEM images of MWCNT/Nafion/MWCNT materials before and after radiation, (c) pre-radiation, (e) 100 kGy 21% O_2 and 300 kGy 21% O_2, (f) 100 kGy 100% N_2 and 300 kGy 100% N_2, and (d) agglomeration caused by irradiation.

environment of 100 kGy 21% O_2 and 300 kGy 21% O_2, respectively. It can be seen that the MWCNT has obvious agglomeration and fracture, and the agglomeration is more serious with the increase in irradiation dose. The reason for this phenomenon is the generation of many reactive particles, especially oxidative ones, by irradiation splitting under high-energy gamma rays. These active particles will physically and chemically react with the carbon nanotubes through electronic excitation and ionization and displace the carbon atoms by colliding with the carbon atoms on the surface of the carbon nanotubes, resulting in defects in the carbon tubes, which eventually lead to the rupture and agglomeration of the multi-walled carbon nanotubes on the surface of the composite film. However, it is revealed from Figure 5(f) that, in a 100% N_2 radiation atmosphere, the surface microstructure of the composite films has hardly changed compared to pre-radiation, which corresponds to the conclusion of the surface resistance experiment.

Figure 6 shows the XRD spectra of composite film, which indicates whether the structural composition of the core layer and the electrode layer changes. Figure 6(a) shows that significant graphite diffraction peaks appear in the electrode layers of the five composite films at 2θ = 25.8°, corresponding to the (002) crystal plane. And there is no change among the d_{002} of the five electrode layers, indicating that under different irradiation conditions, the crystal structure of graphite diffraction peak (002) has not changed conspicuously, and no amorphous carbon is produced. It can be seen from Figure 6(b) that the core layer shows two obvious characteristic diffraction peaks at 2θ = 23 and 38°, which are,

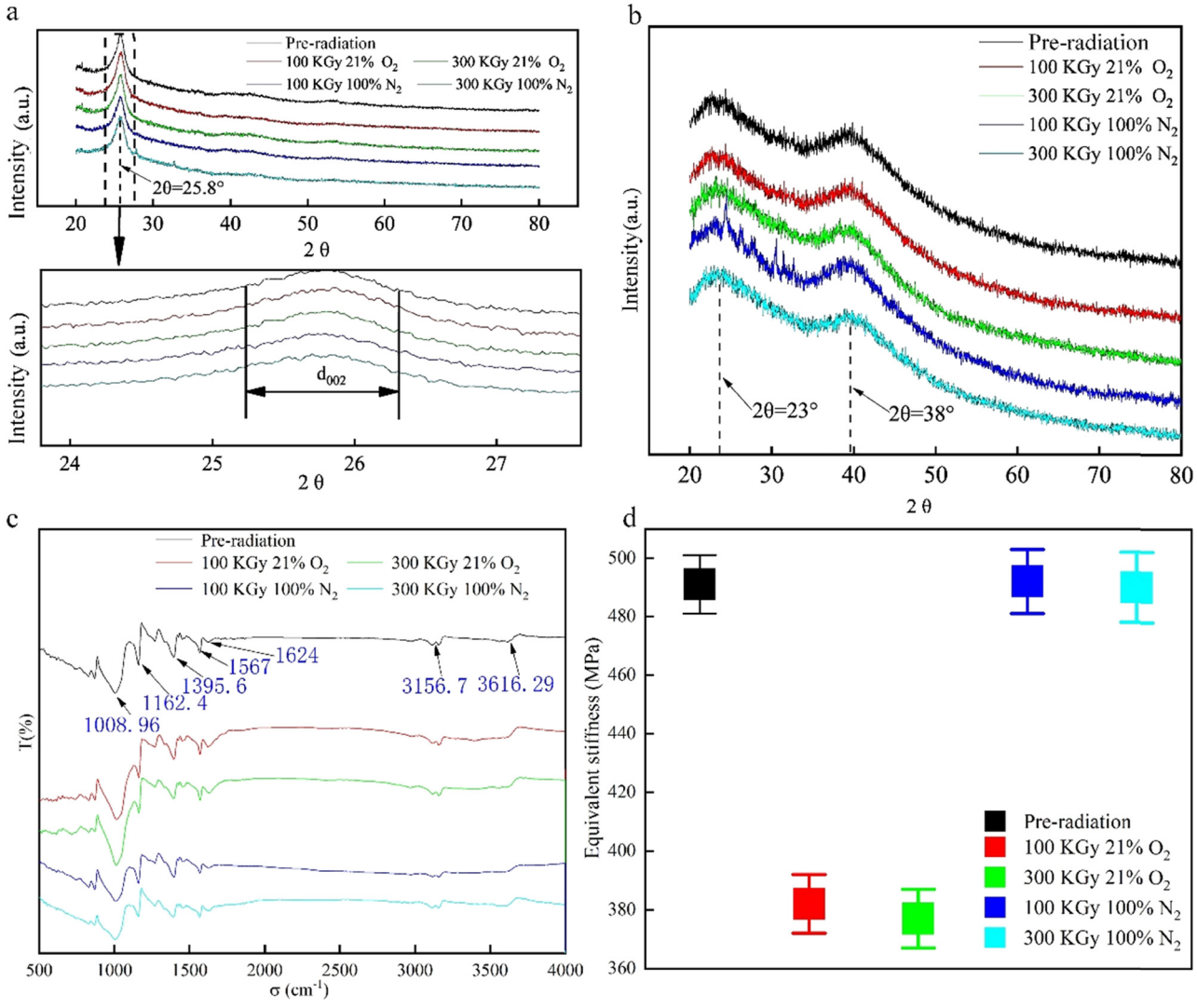

Figure 6: Properties of the composite film before and after radiation. (a) The XRD spectra of electrode layer, (b) core layer, (c) FT-IR pattern of the composite film, and (d) equivalent stiffness of the composite film.

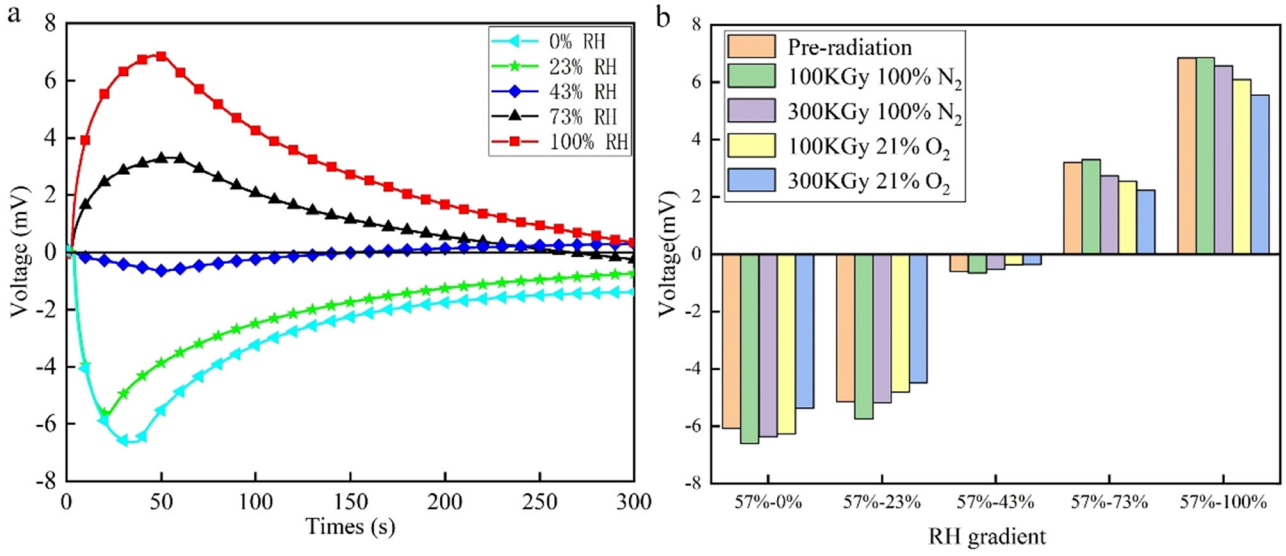

Figure 7: Humidity–voltage response curve of MWCNT/Nafion/MWCNT humidity sensing film (a) after 100 kGy radiation in 100% N_2 atmosphere from 57% RH humidity to other humidity. (b) The corresponding amplitude of voltage of each sample piece under different humidity changes.

respectively, the characteristic peaks of ionic liquid ($EMIBF_4$) and Nafion. The characteristic peak did not change after irradiation, indicating that the MWCNT had a certain shielding effect in the gamma-ray irradiation environment, and high-energy gamma rays did not penetrate the electrode layer to change the structural composition of the core layer.

The infrared spectrum test results of the composite films are shown in Figure 6(c), which have a little difference after radiation. All FTIR spectra of composite films include a broad band at 3,616 cm^{-1}, indicating the characteristic stretching vibrations of hydroxyl (O–H) bonds. In 21% O_2 radiation atmosphere, the peak (O–H) intensity of the composite films, radiated by 100 and 300 kGy, is higher than that of the non-radiated composite films, which indicates that the number of oxygen-containing groups increases on the surface of the composite films, and a small number of functional groups have been presented before radiation. Further, a weak C═O bond stretching vibration signal appears near 1,624 cm^{-1}, and it can be seen that after irradiation in 21% O_2 atmosphere, the peak position at this place is significantly enhanced and the peak width is increased, indicating that high-energy γ-ray irradiation leads to increased structural defects on the surface of the composite membrane and connects more carboxyl functional groups. However, after irradiation in 100% N_2 atmosphere, the characteristic peak of the composite film does not change, which indicates that the film has better radiation resistance under 100% N_2 irradiation environment. The peaks at 3,156.7 and 1,567 cm^{-1} represent the imidazole ring and $–CH_3$ in the ionic liquid (EMIBF4), respectively. It can also be seen from the figure that the peak intensity changed after irradiation in 21% O_2 atmosphere. Similarly, under 21% O_2 atmosphere irradiation, the characteristic C–F peaks at 1,162.4 and 1,008.96 cm^{-1} were significantly enhanced, and the width of the peak increased. The reason for this phenomenon is that high-energy γ-rays destroy the PVDF molecular structure on the surface of the composite membrane, leading to changes in its characteristic peak.

Figure 6(d) shows the equivalent elastic modulus of the composite film by the free attenuation method to detect the effect of radiation on its mechanical properties. The elastic modulus of the composite film before radiation is 493 MPa. When the film is irradiated in 21% O_2, the elastic modulus of the composite film decreased significantly to 383 and 377 MPa after 100 and 300 kGy γ-rays irradiation, because the fracture of the MWCNT on the surface of the composite film led to the decrease of both its stiffness and hardness. However, under 100% N_2 irradiation atmosphere, the elastic modulus is, respectively, 492 and 490 MPa, which means that the mechanical properties of the composite film do not change under 100% N_2 irradiation atmosphere.

Figure 7(a) shows the humidity response at different humidity gradients of the composite film after 100 kGy radiation in 100% N_2 atmosphere. It exhibits relaxed characteristics of a slow recovery after a quick rise, which is very similar to the sensing process of ion-exchange polymer metal composite (24). When the composite film is in a certain humidity state (57% RH, for example) for a long time (over 24 h), the water molecules inside the composite film and the moisture of the ambient humidity will

exchange until a dynamic equilibrium is reached. After the high-humidity or low-humidity gas is charged, the equilibrium state will be broken. Then, the abundant water molecules in the environment will be exchanged into the composite film or the water molecules inside the composite film will go through the electrode layer into the surroundings, which causes the anisotropic swelling of the composite film and in turn forces the water molecules to drag and move the ions to migrate along the direction of the strain gradient, finally resulting the produce of electrical signal. To reveal the influence of radiation on the humidity response performance, we compared the corresponding amplitude of voltage of each sample piece under different humidity changes in Figure 7(b). There was a significant attenuation of the maximum value of the voltage response of the irradiated sample in the aerobic environment compared with the non-irradiated sample, which indicates that the high energy γ-ray has destroyed the surface structure of the composite film in 21% O_2 radiation atmosphere, leading to the voltage response valve decline. Furthermore, the voltage response value decreased with the increase in radiation intensity. However, in 100% N_2 radiation atmosphere, the voltage response amplitude did not decrease due to radiation and even increased to a certain extent under 100 kGy radiation in 100% N_2 atmosphere, which indicated that the composite membrane had excellent radiation resistance in the anaerobic environment.

4 Conclusion

In this work, we have successfully demonstrated the possibility of obtaining high-performance radiation-resistant composite films using MWCNT. A novel radiation-resistant composite film consisting of an inner layer of Nafion/ILs and electrode layers of MWCNT/PVDF/ILs was prepared by a laminated hot-pressing process. The following conclusions were derived from radiation exposure experiments in various environments: (1) destruction of composite films by radiation is primarily dependent on the presence or absence of oxygen in the air. The radiation irradiation in normal air (containing 21% O_2) results in elevated surface resistance of the composite membrane, increased modulus of elasticity, and deteriorated humidity response performance. Conversely, under an oxygen-free environment consisting of 100% N_2, the performance of the composite membrane remains constant. (2) The main reason for the significant performance degradation is MWCNT agglomeration in the composite film. In normal air, as the irradiance rises, the MWCNT agglomeration in the composite film increases, resulting in significant performance degradation.

Acknowledgments: This research was supported by the Young Talent Lift Project (19JZ-12KW-42), the Natural Science Foundation of China (51975184), and the National Key Research and Development Program of China (2019YFB1311600). The authors gratefully acknowledge the supports.

Author contributions: Junjie Sheng: methodology, conceptualization, methodology, software, technical support; Yujun Ji: validation, formal analysis, data curation, writing – original draft, drawings; Shijie Zhao: data curation, writing – original draft, drawings; Yong Qiu: supervision, funding acquisition, writing – review & editing; Chun Zhao: methodology, writing – review & editing; Gangqiang Tang: methodology, writing – review & editing; Yanjie Wang: supervision, project administration, funding acquisition.

Conflict of interest: No potential conflict of interest was reported by the authors.

Data availability statement: The data that support the findings of this study are available from the corresponding author, upon reasonable request.

References

(1) Lei D, Zhang Q, Liu N, Su T, Wang L, Ren Z, et al. Self-powered graphene oxide humidity sensor based on potentiometric humidity transduction mechanism. Adv Funct Mater. 2022;32(10):2107330.
(2) Akram R, Yaseen M, Farooq Z, Rauf A, Almohaimeed ZM, Ikram M, et al. Capacitive and conductometric type dual-mode relative humidity sensor based on 5, 10, 15, 20-tetra phenyl porphyrinato nickel(II)(TPPNi). Polymers. 2021;13(19):3336.
(3) Zhuang Z, Li Y, Li X, Zhao C. A novel polymer-salt complex based on LiCl doped SPEEK/poly (ether ether ketone)-co-poly (ethylene glycol) for humidity sensors. IEEE Sens J. 2021;21(7):8886–95.
(4) Andriianova AN, Salikhov RB, Latypova LR, Mullagaliev IN, Salikhov TR, Mustafin AG. The structural factors affecting the sensory properties of polyaniline derivatives. Sustain Energy Fuels. 2022;6(14):3435–45.
(5) Li J, Zhang J, Sun H, Hong D, Li L, Yang Y, et al. An optical fiber relative humidity sensor based on hollow-core fiber and hydroxypropyl methylcellulose hydrogel film. Optik. 2019;195:163172.
(6) Kang TG, Park JK, Kim BH, Lee JJ, Choi HH, Lee HJ, et al. Microwave characterization of conducting polymer PEDOT: PSS film using a microstrip line for humidity sensor application. Measurement. 2019;137:272–7.
(7) Kumar A, Gupta G, Bapna K, Shivagan DD. Semiconductor-metal-oxide-based nano-composites for humidity sensing applications. Mater Res Bull. 2022;158:112053.

(8) Ishizaki R, Katoh R. Fast-response humidity-sensing films based on methylene blue aggregates formed on nanoporous semiconductor films. Chem Phys Lett. 2016;652:36–9.
(9) Tang F, Li Y, Zeng B, Liu G, Zhao J, Chen L. Lamellar nanocomposite based on a 1D Crayfish-like CeIII-Substituted Phospho(III) tungstate semiconductor and polyaniline used as a high-performance humidity sensing device. ACS Appl Mater Interfaces. 2022;14(43):48876–87.
(10) Mandić V, Bafti A, Pavić L, Panžić I, Kurajica S, Pavelić JS, et al. Humidity sensing ceria thin-films. Nanomaterials. 2022;12(3):521.
(11) Farzaneh A, Mohammadzadeh A, Esrafili MD, Mermer O. Experimental and theoretical study of TiO2 based nanostructured semiconducting humidity sensor. Ceram Int. 2019;45(7):8362–9.
(12) Abdulameer AF, Suhail MH, Abdullah OG, Al-Essa IM. Fabrication and characterization of NiPcTs organic semiconductors based surface type capacitive–resistive humidity sensors. J Mater Sci Mater Electron. 2017;28(18):13472–7.
(13) Jeong Y, Hong S, Jung G, Shin W, Park J, Kim D, et al. Highly stable Si MOSFET-type humidity sensor with ink-jet printed graphene quantum dots sensing layer. Sens Actuators B Chem. 2021;343:130134.
(14) Hou M, Wang N, Chen Y, Ou Z, Chen X, Shen F, et al. Laser-induced graphene coated hollow-core fiber for humidity sensing. Sens Actuators B Chem. 2022;359:131530.
(15) Garg A, Almáši M, Bednarčík J, Sharma R, Rao VS, Panchal P, et al. Gd(III) metal-organic framework as an effective humidity sensor and its hydrogen adsorption properties. Chemosphere. 2022;305:135467.
(16) Liu X, Huang D, Lai C, Zeng G, Qin L, Wang H, et al. Recent advances in covalent organic frameworks (COFs) as a smart sensing material. Chem Soc Rev. 2019;48(20):5266–302.
(17) Chen T, Zhang D, Tian X, Qiang S, Sun C, Dai L, et al. Highly ordered asymmetric cellulose-based honeycomb membrane for moisture-electricity generation and humidity sensing. Carbohydr Polym. 2022;294:119809.
(18) Zhang Y, Zhang W, Li Q, Chen C, Zhang Z. Design and fabrication of a novel humidity sensor based on ionic covalent organic framework. Sens Actuators B Chem. 2020;324:128733.
(19) Kim Y, Baek J, Kim S, Kim S, Ryu S, Jeon S, et al. Radiation resistant vanadium-graphene nanolayered composite. Sci Rep. 2016;6:24785.
(20) Si S, Li W, Zhao X, Han M, Yue Y, Wu W, et al. Significant radiation tolerance and moderate reduction in thermal transport of a tungsten nanofilm by inserting monolayer graphene. Adv Mater. 2017;29:1604623.
(21) Al-Haik M, Pham TT, Skandani AA, Bond J, El-Genk MS. Effect of the chirality on the radiation induced damage of carbon nanotubes/polyethylene composites: a molecular dynamics approach. J Comput Theor Nanosci. 2015;12(2):270–9.
(22) Li H, Tang XB, Chen FD, Huang H, Liu J. Molecular dynamics study of radiation damage and microstructure evolution of zigzag single-walled carbon nanotubes under carbon ion incidence. Nucl Instrum Methods B. 2016;378:31–7.
(23) Luo M, Zhu M, Wei M, Shao S, Robin M, Wei C. Radiation-hard and repairable complementary metal-oxide-semiconductor circuits integrating n-type indium oxide and p-type carbon nanotube field-effect transistors. ACS Appl Mater Interfaces. 2020;12(44):49963–70.
(24) Wang Y, Tang G, Zhao C, Wang K, Wang J, Ru J, et al. Experimental investigation on the physical parameters of ionic polymer metal composites sensors for humidity perception. Sens Actuators B Chem. 2021;345:130421.